crystals

MDPI

Article

Synthesis, X-ray Single Crystal, Conformational Analysis and Cholinesterase Inhibitory Activity of a New Spiropyrrolidine Scaffold Tethered Benzo[*b*]Thiophene Analogue

Assem Barakat [1,2,*], Saied M. Soliman [2], Saeed Alshahrani [1], Mohammad Shahidul Islam [1], M. Ali [1], Abdullah Mohammed Al-Majid [1] and Sammer Yousuf [3]

1 Department of Chemistry, College of Science, King Saud University, P.O. Box 2455, Riyadh 11451, Saudi Arabia; chemistry99y@gmail.com (S.A.); mislam@ksu.edu.sa (M.S.I.); maly.c@ksu.edu.sa (M.A.); amajid@ksu.edu.sa (A.M.A.-M.)

2 Department of Chemistry, Faculty of Science, Alexandria University, P.O. Box 426, Ibrahimia, Alexandria 21321, Egypt; saied1soliman@yahoo.com

3 H.E.J. Research Institute of Chemistry, International Centre for Chemical and Biological Sciences, University of Karachi, Karachi 75270, Pakistan; dr.sammer.yousuf@gmail.com

* Correspondence: ambarakat@ksu.edu.sa; Tel.: +966-11467-5901; Fax: +966-11467-5992

Received: 26 December 2019; Accepted: 13 February 2020; Published: 15 February 2020

Abstract: Described herein is a one-pot protocol for the synthesis of a substituted spiropyrrolidine scaffold tethered benzo[*b*]thiophene analogue from (*E*)-3-(benzo[*b*]thiophen-2-yl)-1-(4-fluoro-phenyl)-prop-2-en-1-one. The described protocol has the advantage of the high purity of the cyclized adduct and high chemical yield. To assign the chemical structure, different spectrophotometric tools have been applied, including ^{1}H-NMR, ^{13}C-NMR, FTIR, and the X-ray single crystal technique. The X-ray structure showed that the studied compound exist in two disordered parts with equal partial occupancies. The energies of the two conformers were found to be very similar and not exceed 1 kcal/mol, which justifies their coexistence in the crystal with equal percentage. The molecular packing in the crystal was analyzed using Hirshfeld topology analysis. The packing described as two dimensional hydrogen bond network extended along the *ac*-plane in both conformers but the intermolecular interactions included in each conformer are not similar. The synthesized spiropyrrolidine scaffold tethered benzo[*b*]thiophene analogue was examined against cholinesterase inhibitory activity and show moderate activity compared to standard drug galantamine.

Keywords: spiropyrrolidine; thiazole; benzo[*b*]thiophene; conformational analysis; cholinesterase inhibitory activity

1. Introduction

Alzheimer's disease (AD) treatment is an exciting and interesting research area for chemists. Alzheimer's disease (AD) plays a crucial rule in dementia, affecting millions of people around the world, according to the Alzheimer's World Report [1]. The treatment of Alzheimer's disease symptoms is based on inhibiting the cholinesterase enzymes (ChEs) which exist in the central nervous system [2,3]. To design a new, and safe pharmaceutical drug with long half-live time, high bioavailability, and high efficacy with less toxicity is a challenge in pharmaceutical research.

Spiropyrrolidines scaffold are reported as a lead compound for inhibiting both cholinesterases (ChEs) enzymes including acetylcholinesterase (AChE), and butyrylcholinesterase (BChE) [4,5]. One of the well-known heteroaromatic molecule scaffolds is benzo[*b*]thiophene which possesses

a wide range of pharmaceutical applications, including anti-cancer drugs, and also in the material chemistry applications [6]. Some examples of commercially available compounds that contains the benzo[*b*]thiophene core structure are: raloxifene [7] (trade name: Evista; as anti-cancer agent for breast cancer), sertaconazole [8], zileuton [9] and tamoxifen [10]. Additionally, several reports have disclosed the importance in medicinal chemistry of the benzo[*b*]thiophene scaffold which can act as an inhibitor for acetyl-CoA carboxylase [11], tubulin polymerisation [12,13], and also as a modulator for the estrogen receptor [14]. On the other hand, benzo[*b*]thiophenes have been used as anticonvulsant [15], antidepressant, antidiabetic [16], anti-tubercular [17], anti-fungal [18], enzyme inhibitor [19], and anti-malarial drugs [20], and are used in asthma treatment too [8].

In this paper we combined different pharmacophores including spiroindoline, pyrrole, thiazole, and benzo[*b*]thiophene moieties into one molecule which has been assessed in vitro for its AChE enzyme inhibition for AD treatment. The structure of the newly synthesized compound was confirmed using the single crystal X-ray diffraction technique. Hirshfeld topology analysis of molecular packing was performed to determine the different intermolecular contacts in the crystal structure. DFT calculations were carried out to study the structural aspects of the studied compound.

2. Materials and Methods

2.1. General Methods

"All melting points were determined using a Mel-Temp electrothermal apparatus (Electrothermal, Staffordshire, UK), and are uncorrected. Thin layer chromatography (TLC) was conducted on silica gel (Kieselgel G, Merck, Darmstadt, Germany) and spots were detected under UV light at 254 nm. IR spectra were recorded in a KBr matrix with a Spectrum 100 FT-IR spectrophotometer (Perkin Elmer, Waltham, MA, USA). ^{1}H- and ^{13}C-NMR spectra were recorded in DMSO-d_6 as solvent using a JEOL 400 MHz instrument (JEOL, Ltd, Tokyo, Japan), and the chemical shifts (δ) values are given in ppm. The X-ray crystallographic analysis was performed using the SMART APEX II D8 Venture diffractometer (Bruker D8 Venture, Karlsurehe, Germany) located at Karachi University."

*2.2. Synthesis of 7'-(Benzo[*b*]thiophen-2-yl)-6'-(4-fluorobenzoyl)-1',6',7',7a'-tetrahydro-3'H-spiro[indoline-3,5'-pyrrolo[1,2-c]thiazol]-2-one* (**5**)

A solution of equimolar amounts of (*E*)-3-(benzo[*b*]thiophen-2-yl)-1-(4-fluorophenyl)-prop-2-en-1-one (1.0 mmol), L-4-thiazolidinecarboxylic acid (1.0 mmol) and isatin (1.0 mmol) in methanol (10 mL) was refluxed for 1h. The target product was precipitated and the resulting solid was filtered and recrystallized from DCM/methanol to afford a crystalline compound. Yield 459 mg (0.9 mmol, 90%); m.p.: 101–103 °C; ^{1}H-NMR (DMSO-d_6) δ 10.39 (s, 1H, NH), 7.90 (d, J = 7.6 Hz, 1H, FC_6H_4), 7.77 (d, J = 7.5 Hz, 1H, FC_6H_4), 7.54 (s, 1H, thiophene-H), 7.48–7.27 (m, 5H, oxindole-H and FC_6H_4 & benzothiophene-H), 7.15 (q, J = 8.1, 7.4 Hz, 3H, oxindole and benzothiophene), 6.96 (t, J = 7.6 Hz, 1H, oxindole-H), 6.53 (d, J = 7.9 Hz, 1H, oxindole-H), 4.75 (d, J = 10.7 Hz, 1H, CHCO), 4.33–4.17 (m, 2H, CH_2), 3.73 (d, J = 10.3 Hz, 1H, CH), 3.35 (d, J = 10.3 Hz, 1H, CH), 3.19 (d, J = 6.4 Hz, 2H, CH_2); ^{13}C-NMR (DMSO-d_6) δ 195.09, 178.59, 166.85, 164.34, 143.52, 142.59, 140.07, 138.83, 133.57, 131.13, 130.60, 128.48, 125.14, 124.83, 123.91, 123.15, 122.94, 121.71, 116.25, 110.23, 74.36, 73.97, 62.66, 54.09, 47.07, 36.55; IR (KBr, cm^{-1}) ν_{max} = 3420 (NH), 3066 (CH), 2927(CH), 1704 (C=O), 1597 (C=C), 1472, 1237; [Anal. Calcd. for $C_{28}H_{21}FN_2O_2S_2$: C, 67.18; H, 4.23; N, 5.60; Found: C, 67.01; H, 4.39; N, 5.73]; LC/MS (ESI, *m/z*): [M+], found 511.10, $C_{28}H_{21}FN_2O_2S_2$ for 510.10.

2.3. Single-Crystal X-ray Diffraction Analysis

Single-crystal X-ray diffraction analysis of the studied compound was carried out by mounting an appropriate crystal with dimension 0.11 × 0.09 × 0.07 mm^3 on a Bruker D8 Venture instrument equipped with a CCD Photon II detector and graphite monochromator having Cu Kα radiation (λ = 1.54178 Å) at T = 100(2) K for data collection. For the integration, and reduction of data,

SAINT (Bruker 1998) program was used [21]. The solved structure was done by direct method, and Fourier transformation techniques, and further refined by full-matrix least-squares techniques on F^2 using SHELXL-2018 program. PLATON [22], and SHELXL [23] programs were employed for the final refinement of solved structure (Table 1). "The final refinement was carried out by full-matrix least-squares techniques with anisotropic thermal data for non-hydrogen atoms on *F*. CCDC 1972061 contains the supplementary crystallographic data for this compound can be obtained free of charge from the Cambridge Crystallographic Data Centre via www.ccdc.cam.ac.uk/data_request/cif."

Table 1. Experimental and refinement details of compound **5**.

CCDC	1972061
Empirical formula	$C_{29}H_{25}N_2O_3FS_2$
Formula weight	532.63
Temperature	100(2) K
Wavelength	1.54178 Å
Crystal system	Orthorhombic
Space group	P 2_1 2_1 2_1
Unit cell dimensions	a = 8.2588(4) Å b = 10.6003(5) Å, α = β = γ = 90°. c = 28.8478(14) Å
Volume	2525.5(2)Å^3
Z	4
Calculated density	1.401 mg/m^3
Absorption coefficient	2.268 mm^{-1}
F(000)	1112
Crystal size	0.11 × 0.09 × 0.07 mm^3
Theta range for data collection	4.444 to 68.231
Limiting indices	−9 ≤ h ≤ 8, −11 ≤ k ≤ 12, −33 ≤ l ≤3 4
Reflections collected/unique	16366/4587
R(int)	0.0332
Completeness to theta = 67.679	99.5%
Refinement method	Full-matrix least-squares on F^2
Data/restraints/parameters	4587/0/334
Goodness-of-fit on F^2	1.038
Final R indices [I>2sigma(I)]	R1 = 0.0396, wR2 = 0.0970
Final R indexes [all data]	R1 = 0.0418, wR2 = 0.0987
Largest diff. peak and hole	0.41 and −0.36 e.A^{-3}

2.4. Hirshfeld Surface Analysis

"The topology analyses were performed using the Crystal Explorer 17.5 program [24] in order to determine the percentages of the different intermolecular interactions in the crystal structure of the studied compound."

2.5. Computational Methods

All DFT calculations were performed with the Gaussian 09 software package [25,26] using the B3LYP/6-31G(d,p) method. The resulting optimized structures showed no imaginary frequencies.

Natural population analysis was performed using NBO 3.1 program as implemented in the Gaussian 09W package [27].

3. Results and Discussion

3.1. Chemistry

In this paper we describe the synthesis of a substituted spiropyrrolidine scaffold tethered benzo[*b*]thiophene analogue from (*E*)-3-(benzo[*b*]thiophen-2-yl)-1-(4-fluorophenyl)prop-2-en-1-one based on reported methods [28–34]. Initially the chalcone **2** was synthesized based on the benzo[*b*]thiophene scaffold starting from benzo[*b*]thiophene and *p*-fluoroacetophenone (Scheme 1).

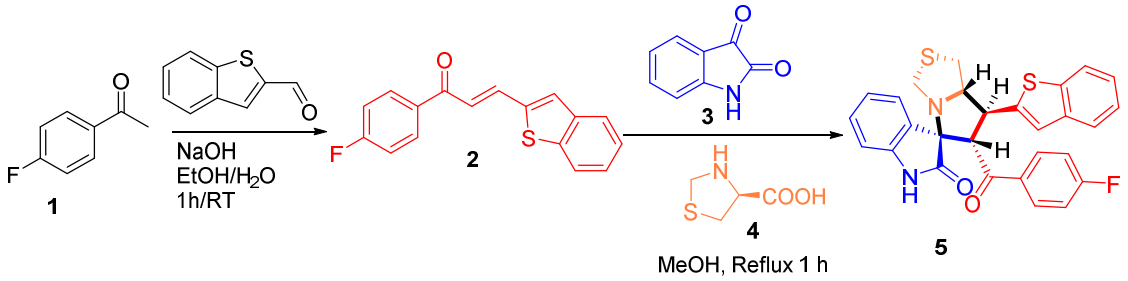

Scheme 1. The synthetic route of compound **5**.

Subsequently, a one pot three component reaction of the synthesized chalcone **2** with isatin **3** and thioproline **4** afforded the cyclized compound **5** in excellent yield, regio- and diasetereoselectivity. Based on the ^{1}H-NMR spectrum, the protons have been assigned as follows: a singlet for the NH proton appears at δ 10.39 ppm and the 13 aromatic protons appeared as expected in the aromatic region, along with signals in the lower field chemical shift region between δ 4.75 until 3.19 ppm, that could be assigned for the protons belonging to fused pyrrolothiazole ring. The ^{13}C-NMR signals are also consistent with the assigned carbons. The FTIR spectrum shows characteristic peaks, including NH (3420), CH (3066, 2927), CO (1704) and C=C (1597) functionalities. Additionally, a suitable single crystal was grown and submitted for single crystal X-ray diffraction analysis and the data is reported here (an image of the single crystal and the ORTEP structure are shown in Figure 1).

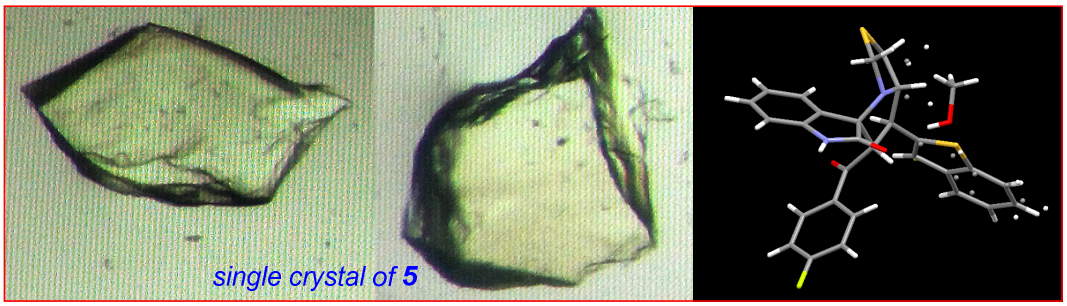

Figure 1. Single crystal and 3D structure of compound **5**.

The relative configuration of the synthesized substituted spiropyrrolidine scaffold was assigned by the help of the X-ray single crystal technique, and a plausible reaction mechanism is shown in Scheme 2 [28–34]. The reaction proceeds following a one pot multicomponent protocol in which initially isatin reacted with thioproline to afford an intermediate that leads to an azomethine yilde after expulsion of carbon dioxide. Subsequently the azomethine yilde reacts with the chalcone to provide the target compound in a regioselective and diastereoselective manner. The reaction proceeds regioselectively via path A to afford the regioisomeric product **5**, while the second regioisomers **5** is

not formed (path B). There are possible diastereoselective products that could be formed but in this case the only diastereoselective compound **5** was observed (path C).

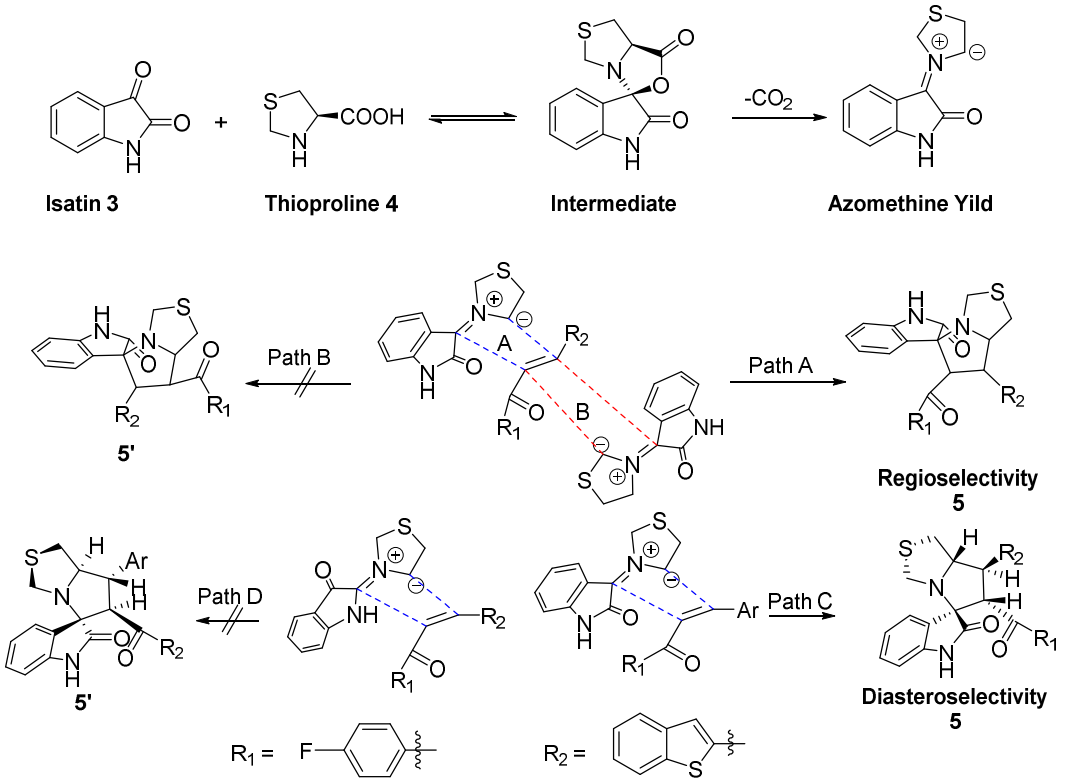

Scheme 2. Plausible reaction mechanism for the synthesized compound.

3.2. Crystal Structure Discription

Crystallographic data and refinement details for the studied compound, $C_{28}H_{21}FN_2O_2S_2.CH_3OH$ are listed in Table 1. The compound $C_{28}H_{21}FN_2O_2S_2$ co-crystallized with one methanol molecule as crystallization solvent. It crystallizes as block colorless crystals in the orthorhombic crystal system and has the $P2_12_12_1$ as a space group. The asymmetric unit comprised one molecular unit and Z = 4. A list of geometric parameters (bond distances and angles) is given in Table S1 (Supplementary Data). It is clear from the X-ray structure analysis that the compound has disorder over two positions as shown in Figure 2. The difference between the two conformers is a result of two types of disorder which are rotational, and positional disorders of the benzothiophene, and thiophene ring, respectively with partial occupancies of (50%:50%) for each, as shown in Figure 2. The interesting point is the disorder of the benzothiophene moiety in which the structure exhibited the two conformational structures indicated in the lower part of Figure 2. The main difference between the two conformations is that the benzothiophene moiety is rotated around the C12–C8 bond by 130°.

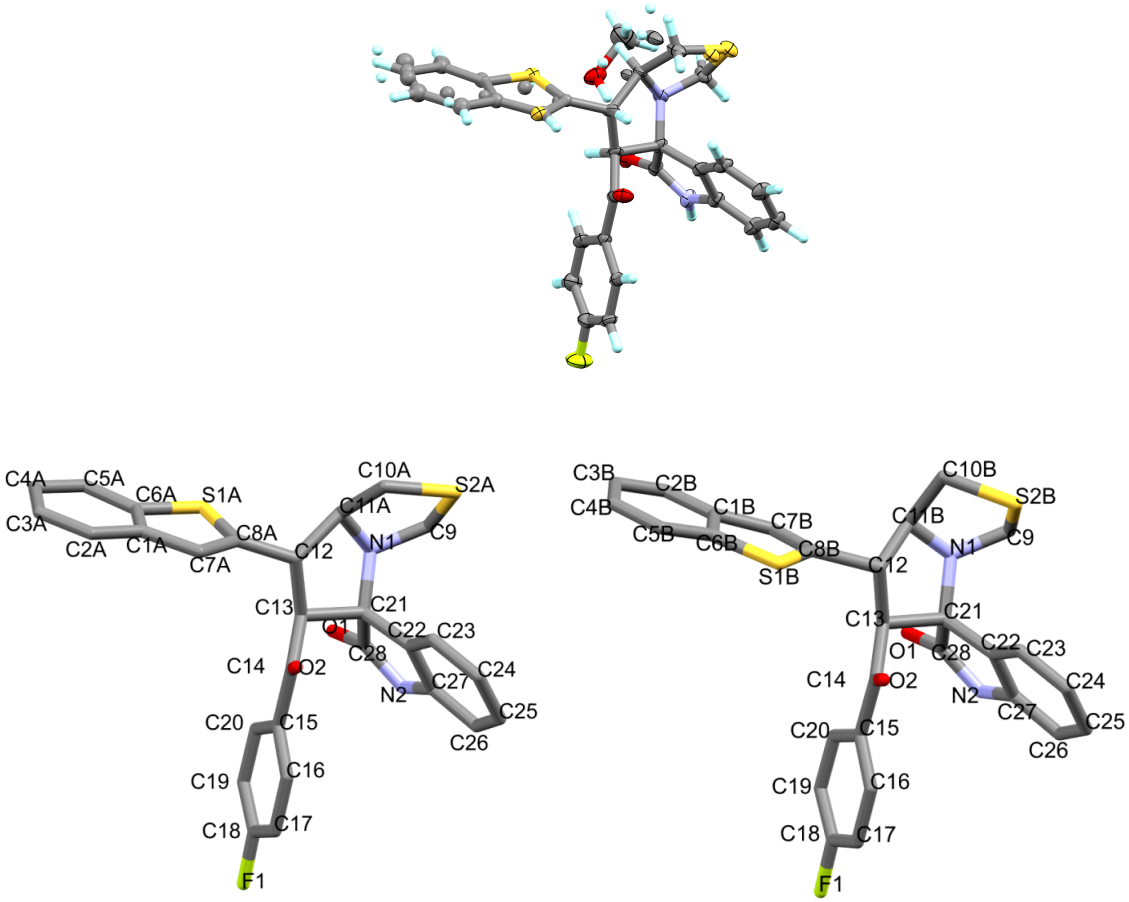

Figure 2. ORTEP structure of **5** showing the disordered system over two positions with equal partial occupancies at 50% probability level (upper) and the atom numbering of each part (lower) showing the two conformers of the studied system where hydrogen atoms and the methanol molecule were omitted for better clarity.

3.3. Crystal Packing

Another interesting difference between the two conformers, which is the intermolecular hydrogen bonding interactions, occurred in each part which are not typically the same. The detailed list of the hydrogen bonding interactions is given in Table 2 while the packing diagram showing the most important hydrogen bonding interactions is shown in Figure 3. In this illustration, the weak C-H. . . O hydrogen bonding interactions are omitted for simplicity.

Table 2. Hydrogen bond distances (Å) and angles (°) in **5**.

D-H ··· A	d(D-H)	d(H ··· A)	d(D ··· A)	<(DHA)
N2-H2. . . O3	0.88	1.96	2.830(3)	172
O3-H3O. . . O1	0.84	1.97	2.775(3)	160
C7A-H7AA. . . S2A	0.95	2.84	3.604(16)	139
C7B-H7BA. . . F1	0.95	2.35	3.080(9)	133
C4B-H4B. . . S1B	0.95	2.84	3.738(8)	158
C10A-H10A. . . S2A	0.99	2.50	3.378(7)	147
C17-H17. . . O1	0.95	2.56	3.368(4)	143
C26-H26. . . O1	0.95	2.55	3.435(4)	154

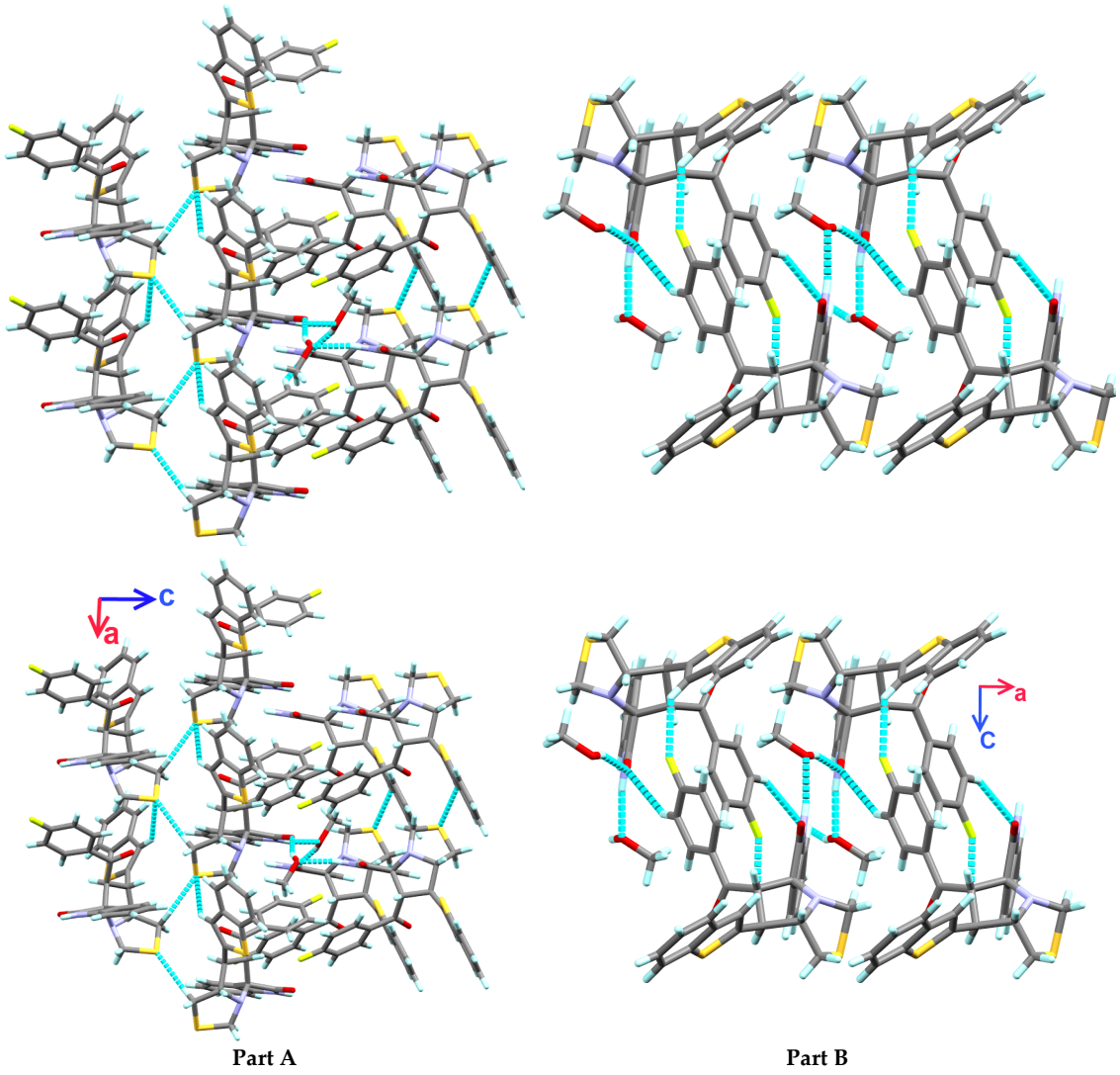

Figure 3. Crystal packing diagram of conformers **A** and **B** of **5**. The turquoise dotted lines represent the N-H . . . O, O-H . . . O, C-H . . . F, C-H . . . S and C-H...O intermolecular interactions.

It is clear that, the packing of the molecular units of part A could be described as a two- dimensional hydrogen bond network extended in the *ac* plane via N2-H2. . . O3 and O3-H3O. . . O1 hydrogen bonds in addition to the weak C7A-H7AA. . . S2A and C10A-H10A. . . S2A intermolecular interactions, with donor acceptor distances of 2.830(3), 2.775(3), 3.604(16) and 3.378(7) Å, respectively. On the other hand, the packing in the second conformer (part B) represent also two dimensional hydrogen bond polymer extended along the *ac*-direction. In addition to the N2-H2. . . O3 and O3-H3O. . . O1 hydrogen bonds, the molecular units are packed via weak C7B-H7BA. . . F1 and C4B-H4B. . . S1B intermolecular interactions with donor acceptor distances of 3.080(9) and 3.738(8) Å, respectively.

3.4. Hirshfeld Analysis of the Molecular Packing

Based on the single crystal X-ray structure of the studied compound, there are two possible conformers for this molecule represented by parts A and B in Figure 4. The Hirshfeld surface mapped over d_{norm}, shape index (SI) and curvedness for this molecule is shown in Figure 5. Decomposition analysis of the different intermolecular contacts indicated that both parts have almost similar intermolecular contacts (Figure 6). The H. . . H, O. . . H, S. . . H, and F. . . H contacts contributed by 44.2%, 11.8%, 9.4%, and 5.9%, respectively for conformer A and 42.5%, 12.4%, 11.4% and 6.8% for conformer B, respectively. Those are the most abundant contacts in the structure of the studied systems.

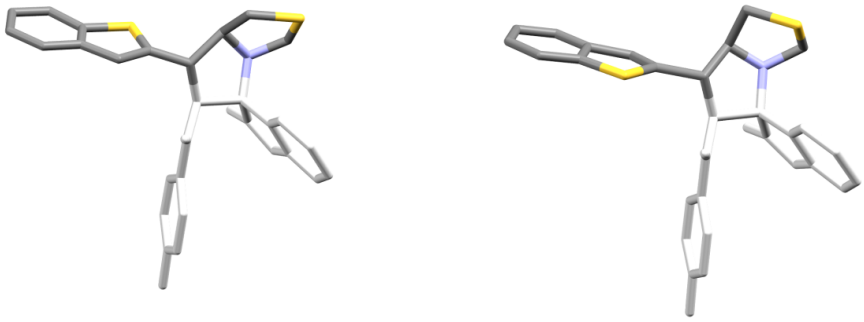

Figure 4. The structure of conformers **A** and **B** as reported by the disorder model in the X-ray structure. The fixed part is made in light grey color and the methanol molecule was omitted for more clarity.

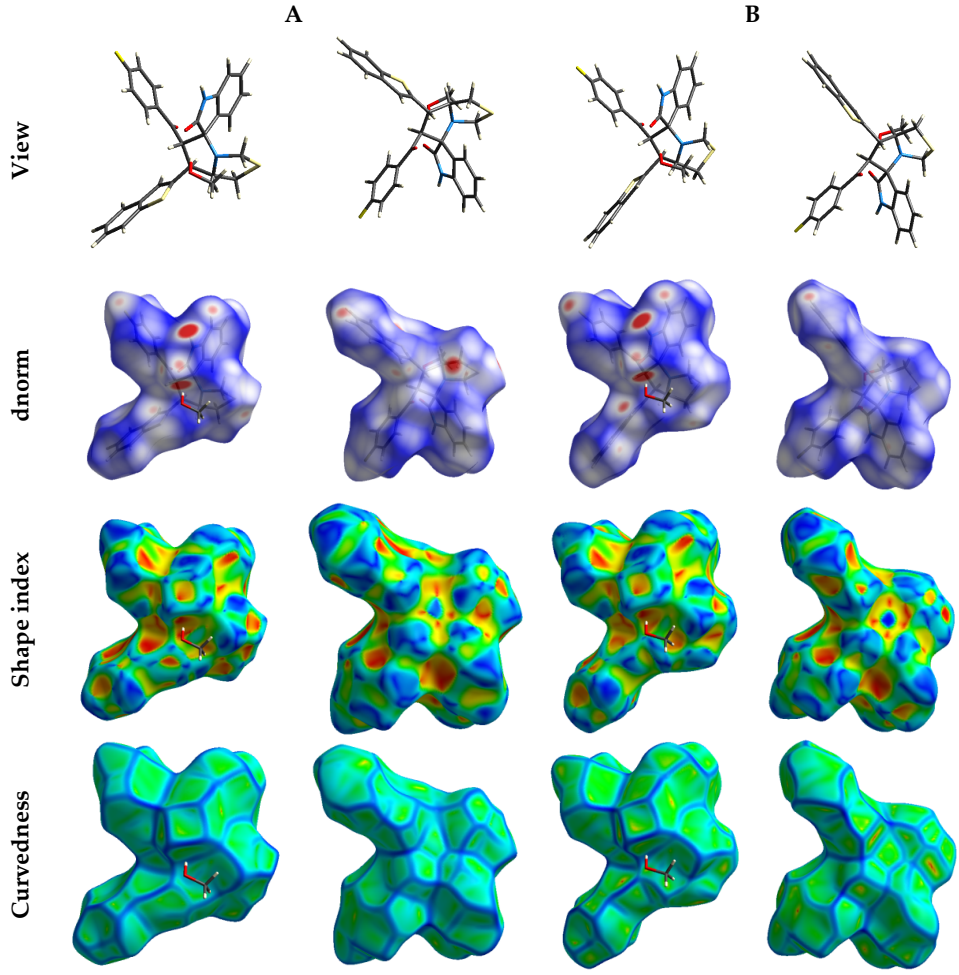

Figure 5. Hirshfeld surfaces mapped over d_{norm}, shape index and curvedness.

As clearly indicated from the decomposed fingerprint of the most common contacts shown in Figure 7, the O. . . H hydrogen bonds are significantly strong in both conformers. The shortest O. . . H contacts are the O3-H3O. . . O1 and N2-H2. . . O3 ones with hydrogen-acceptor distances of 1.838 and 1.828 Å, respectively in both conformers. On other hand, the F. . . H contacts appeared stronger in conformer B than conformer A. The C7B-H7BA. . . F1 has hydrogen-acceptor distance of 2.262 Å while the corresponding value in conformer A for the C13-H13. . . F1 interaction is 2.648 Å. The latter is longer than the van der Waals radii sum of fluorine and hydrogen atoms (2.56 Å). In contrast, the S. . . H contacts are shorter in conformer A than conformer B. In the former there are three significant S. . . H interactions

which are the C10A-H10A. . . S2A, C12-H12 . . . S2A and C7A-H7AA. . . S2A with hydrogen acceptor distances of 2.426, 2.865 and 2.738 Å, respectively. In the conformer B, the weak C10B-H10D. . . S1B, C12-H12. . . S2B and C9A-H9A. . . S1B intermolecular interactions have longer S. . . H contact distances of 2.964, 2.963, and 2.944 Å, respectively. Interestingly, the Hirshfeld analysis detected very small amount (1.3%) of significantly short S . . . F interactions with F1. . . S1A distance of 3.172 Å. The shape index and curvedness maps revealed the absence of significant ring π-π stacking interactions.

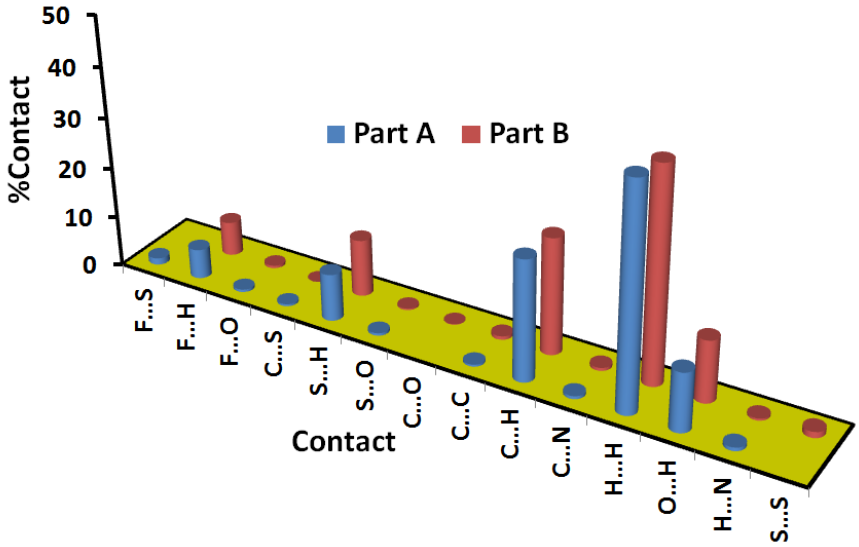

Figure 6. Summary of the intermolecular interactions and their percentages in the crystal structure of the studied compound.

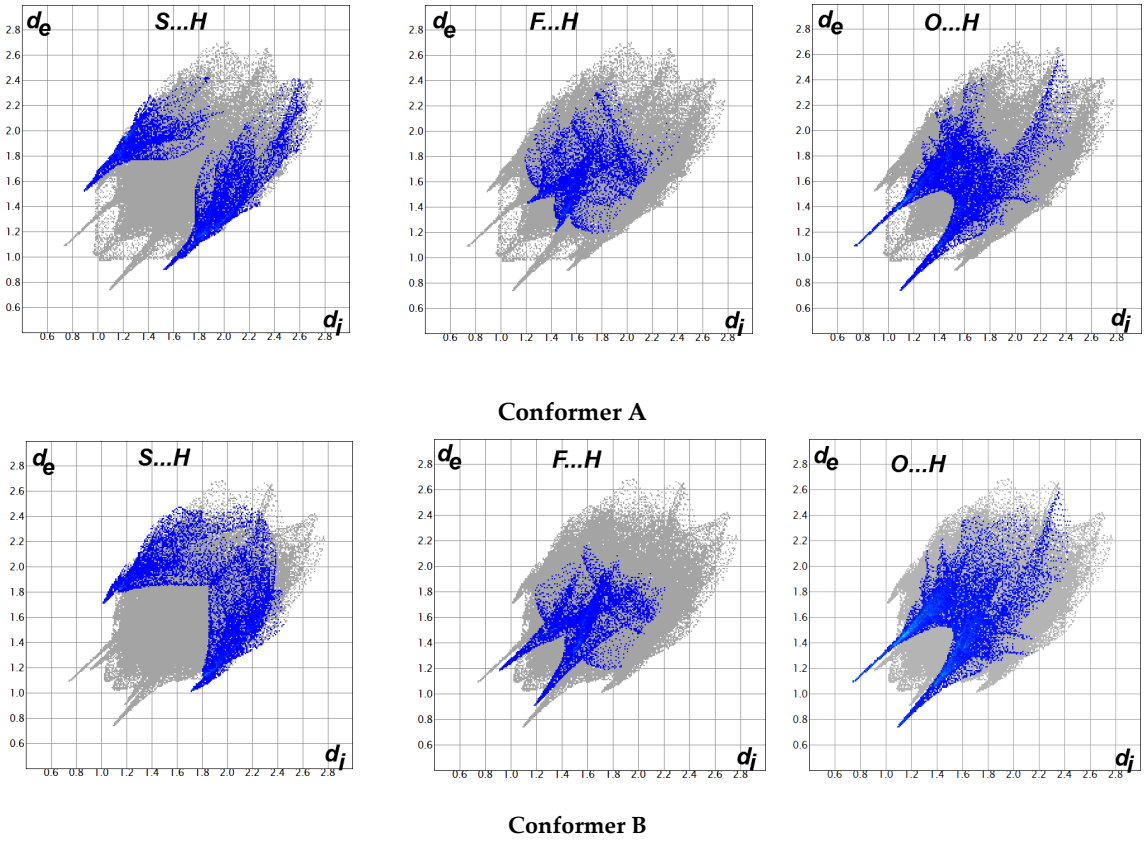

Figure 7. The decomposed fingerprint plots of the most important intermolecular contacts in the crystal structure of the studied compound.

3.5. DFT Studies

The crystal structures of both conformers A and B were optimized using B3LYP method and their total energies are listed in Table 3. It is clear from the results listed in this table that the energy difference is very small. It is found that conformer B is slightly more stable than conformer A by 0.4885 kcal/mol. Further, optimization of the structures of both conformers in absence of methanol as crystallized solvent gave almost the same results (0.6255 kcal/mol) indicating that both conformers have very close stability and could exist in very similar proportions to each other. Also, the crystallization solvent has a little effect on the solid state conformation. The X-ray structure analysis supported this point where the two parts have almost equal partial occupancies. Not only the structures of A and B are energetically very similar but also their polarities are close to each other. The calculated dipole moment values of the two conformers were predicted to be 2.6886 and 2.5838 Debye for conformers A and B, respectively. The solvated species have also close polarities of 3.6435 and 4.3095 Debye, respectively. Similar observation could be noted for the frontier molecular orbital energies (Table 3). The reactivity indices [35–43] of both conformers such as ionization potential (I), electron affinity (A), chemical potential (μ), hardness (η), softness (S), and electrophilicity (ω) indices were calculated based on the HOMO and LUMO energies and were found very close to each other (Table 3). These descriptors could be used to understand the pharmacological and biological reactivity of the compounds.

Table 3. Total energies ($E_{tot.}$), zero point energy correction (ZPVE) and the frontier molecular orbital energies of the studied systems.

Energy	A [a]	A	B [a]	B
$E_{tot.}$	−2235.837	−2351.580	−2235.838	−2351.581
ZPVE	0.430	0.483	0.430	0.483
E_{corr} [b]	−2235.407	−2351.097	−2235.408	−2351.097
HOMO	−5.852	−5.765	−5.640	−5.599
LUMO	−1.782	−1.711	−1.696	−1.710
I	5.852	5.765	5.640	5.599
A	1.782	1.711	1.696	1.710
η	4.071	4.054	3.944	3.889
μ	−3.817	−3.738	−3.668	−3.654
S	0.246	0.247	0.254	0.257
ω	1.790	1.723	1.705	1.717

[a] without methanol [b] $E_{corr} = E_{tot.}$ + ZPVE.

The optimized structures of the organic molecules were matched with the experimental structure in Figure 8 while the calculated and experimental bond distances and angles are listed in Table S2 (Supplementary Data). The correlation coefficients were found in the range of 0.969–0.983 and 0.940–0.959 for bond distances and angles, respectively, which indicated good agreement between the calculated and experimental results. The natural charge distribution at the different atomic sites were calculated and the results were listed in Table S3 (Supplementary Data). The S-atoms have a positive natural charge where the benzothiophene S-atom is more electropositive than that in the thioproline moiety. In contrast, the oxygen atoms are electronegative with natural charges ranging from −0.5487 to −0.6354 e. The most important conclusion that could be concluded from this table is that the methanol molecule has a net charge density of −0.0167 and −0.0178 e for A and B, respectively. The rest organic fragments have the opposite of these values. As a result of the hydrogen bonding interactions, methanol molecule is acting as an electron acceptor while the organic fragments acts as electron donor.

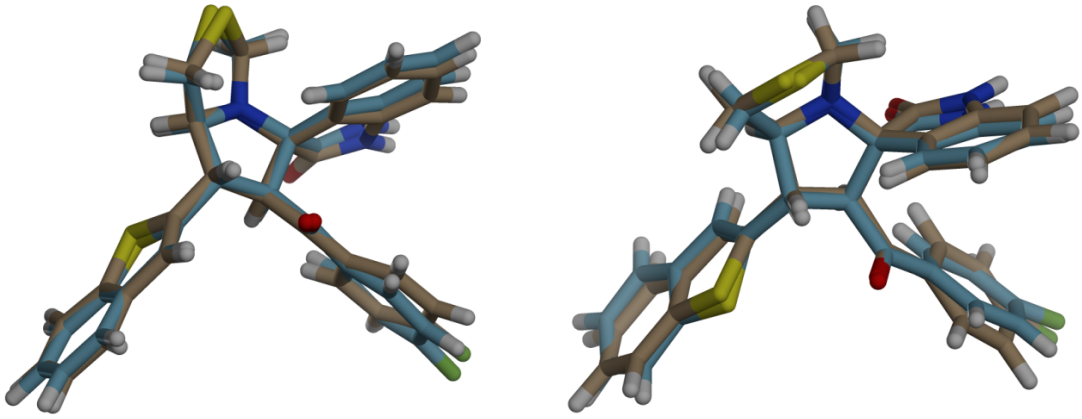

A **B**

Figure 8. Structure matches of the optimized and calculated structures of conformers A and B in the studied organic compound.

3.6. Biological Activity

To show the biological activity of the synthesized compound based on the literature survey an assay has been conducted. The cholinesterase inhibitory activity of the synthesized compound was assessed in vitro [44]. The result is summarized in Table 4. The spiropyrrolidine scaffold tethered benzo[*b*]thiophene analogue analogue has an IC_{50} value of 62.25 μg/mL compared to galantamine (IC_{50} = 0.98 μg/mL). This result shown some activity so further studies must be investigated by synthesis of another analogues and report the SAR.

Table 4. Result of AChE inhibitory activity.

Compound	AChE Inhibition IC_{50} µg/mL	AChE Inhibition IC_{50} µM/mL
5	62.25	124.34
Galantamine	0.98	3.4

4. Conclusions

The proceeding study reported the design and synthesis of spiropyrrolidine scaffold tethered benzo[*b*]thiophene analogue **5** as a potential AChe inhibition agent. The structure features of **5** were elucidated using different techniques. The energies of the two conformers observed experimentally based on the disorder model of the X-ray structure of the studied compound are very close, indicating that the two conformers could exist in equal proportions. Different intermolecular interactions were analyzed using Hirshfeld analysis. Also, the dipole moment, frontier molecular orbitals energies, reactivity descriptors and natural atomic charge populations were discussed based on the B3LYP/6-31G(d,p) method. The synthesized spiropyrrolidine-based benzo[*b*]thiophene exhibited moderate activity compared to galantamine as standard. Further investigations are underway in our laboratory.

Supplementary Materials: The following are available online at http://www.mdpi.com/2073-4352/10/2/120/s1, protocol for the Acetylcholinesterase (AChE) inhibitory assay; Figure S1: ^{1}H-NMR of **5** in DMSO-d_6; Figure S2: ^{13}C-NMR of **5** in DMSO-d_6; Figure S3: FTIR of **5** in KBr; Figure S4: Atom numbering of the optimized structures of conformers A and B (see Table S1). Table S1: Selected bond lengths [Å] and angles [deg] for 5; Table S2: The calculated geometric parameters of the studied conformers with and without the crystallized methanol molecule a; Table S3: Natural charge populations at the different atomic sites of the studied conformers.

Author Contributions: Conceptualization, A.B.; Data curation, S.M.S. and S.Y.; Formal analysis, S.A., M.S.I., M.A. and S.Y.; Funding acquisition, A.B.; Investigation, S.A., M.S.I. and M.A.; Methodology, S.A., M.S.I. and M.A.; Software, S.M.S. and S.Y.; Supervision, A.B. and A.M.A.-M.; Validation, A.M.A.-M.; Visualization, A.M.A.-M.;

Writing—original draft, A.B. and S.M.S.; Writing—review & editing, A.B. All authors have read and agreed to the published version of the manuscript

Funding: This research was funded by Deanship of Scientific Research at King Saud University, Research group NO (RGP-257).

Acknowledgments: The authors would like to extend their sincere appreciation to the Deanship of Scientific Research at King Saud University for providing funding to this Research group NO (RGP-257).

Conflicts of Interest: The authors declare no conflict of interest.

References

1. Alzheimer's Association. Alzheimer's Disease Facts and Figures. *Alzheimer's Dement.* **2019**, *15*, 321–387.
2. Genç, H.; Kalin, R.; Köksal, Z.; Sadeghian, N.; Kocyigit, U.M.; Zengin, M.; Gülçin, İ.; Özdemir, H. Discovery of Potent Carbonic Anhydrase and Acetylcholinesterase Inhibitors: 2-Aminoindan β-Lactam Derivatives. *Int. J. Mol. Sci.* **2016**, *17*, 1736. [CrossRef] [PubMed]
3. Topal, F.; Gulcin, I.; Dastan, A.; Guney, M. Novel eugenol derivatives: Potent acetylcholinesterase and carbonic anhydrase inhibitors. *Int. J. Biol. Macromol.* **2017**, *94*, 845–851. [CrossRef] [PubMed]
4. Kia, Y.; Osman, H.; Kumar, R.S.; Murugaiyah, V.; Basiri, A.; Perumal, S.; Wahab, H.A.; Bing, C.S. Synthesis and discovery of novel piperidone-grafted mono-and bis-spirooxindole. *Bioorg. Med. Chem.* **2013**, *21*, 1696–1707. [CrossRef]
5. Kia, Y.; Osman, H.; Kumar, R.S.; Murugaiyah, V.; Basiri, A.; Perumal, S.; Razak, I.A. A facile chemo-, regio-and stereoselective synthesis and cholinesterase inhibitory activity of spirooxindole–pyrrolizine–piperidine hybrids. *Bioorg. Med. Chem. Lett.* **2013**, *23*, 2979–2983. [CrossRef]
6. Keri, R.S.; Chand, K.; Budagumpi, S.; Somappa, S.B.; Patil, S.A.; Nagaraja, B.M. An overview of benzo [b] thiophene-based medicinal chemistry. *Eur. J. Med. Chem.* **2017**, *138*, 1002–1033. [CrossRef]
7. Meixner, C.N.; Aref, M.W.; Gupta, A.; McNerny, E.M.B.; Brown, D.; Wallace, J.M.; Allen, M.R. Raloxifene mproves Bone Mechanical Properties in Mice Previously Treated with Zoledronate. *Calcif. Tissue Int.* **2017**, *101*, 75. [CrossRef]
8. Croxtall, J.D.; Plosker, G.L. Sertaconazole: A review of its use in the management of superficial mycoses in dermatology and gynaecology. *Drugs* **2009**, *69*, 339–359. [CrossRef]
9. Sarret, C.; Pichard, S.; Afenjar, A.; Boespflug-Tanguy, O. Lack of long-term neurologic efficacy of zileuton in Sjogren-Larsson's syndrome. *Neuropediatrics* **2017**, *48*, 205–206.
10. Vogel, V.G.; Costantino, J.P.; Wickerham, D.L.; Cronin, W.M.; Cecchini, R.S.; Atkins, J.N.; Bevers, T.B.; Fehrenbacher, L.; Pajon, E.R.; Wade, J.L.; et al. Effects of tamoxifen vs raloxifene on the risk of developing invasive breast cancer and other disease outcomes: The NSABP study of tamoxifen and raloxifene (STAR) P-2 trial. *JAMA* **2006**, *295*, 2727–2741. [CrossRef]
11. Chonan, T.; Wakasugi, D.; Yamamoto, D.; Yashiro, M.; Oi, T.; Tanaka, H.; Ohoka-Sugita, A.; Io, F.; Koretsune, H.; Hiratate, A. Discovery of novel (4-piperidinyl)-piperazines as potent and orally active acetyl-CoA carboxylase 1/2 non-selective inhibitors: F-Boc and triF-Boc groups are acid-stable bioisosteres for the Boc group. *Bioorg. Med. Chem.* **2011**, *19*, 1580–1593. [CrossRef] [PubMed]
12. Pinney, K.G.; Bounds, A.D.; Dingeman, K.M.; Mocharla, V.P.; Pettit, G.R.; Bai, R.; Hamel, E. A new anti-tubulin agent containing the benzo [b] thiophene ring system. *Bioorg. Med. Chem. Lett.* **1999**, *9*, 1081–1086. [CrossRef]
13. Romagnoli, R.; Baraldi, P.G.; Carrion, M.D.; Cara, C.L.; Preti, D.; Fruttarolo, F.; Pavani, M.G.; Tabrizi, M.A.; Tolomeo, M.; Grimaudo, S.; et al. Synthesis and biological evaluation of 2-and 3-aminobenzo [b] thiophene derivatives as antimitotic agents and inhibitors of tubulin polymerization. *J. Med. Chem.* **2007**, *50*, 2273–2277. [CrossRef] [PubMed]
14. Lee, K.C.; Moon, B.S.; Lee, J.H.; Chung, K.H.; Katzenellenbogen, J.A.; Chi, D.Y. Synthesis and binding affinities of fluoroalkylated raloxifenes. *Bioorg. Med. Chem.* **2003**, *11*, 3649–3658. [CrossRef]
15. Zaher, A.F.; Khalil, N.A.; Ahmed, E.M. Synthesis and anticonvulsant activity of new 3′-aryl-7-bromo-spiro[[1]benzothiophene-3,2′-[1,3] thiazolidine]-2,4′-dione derivatives. *Orient. J. Chem.* **2010**, *26*, 1241–1248.
16. Moinet, G.; Leriche, C.; Kergoat, M. Antidiabetic Compounds Comprising Benzofuran and Benzothiophene Derivatives. EP1685121 A1. PCT/EP2004/012075, 11 June 2008.
17. Rao, G.K.; Subramaniam, R. Synthesis, antitubercular and antibacterial activities of some quinazolinone analogs substituted with benzothiophene. *Chem. Sci. J.* **2015**, *6*, 92–96. [CrossRef]

18. Jagtap, V.A.; Agasimundin, Y.S. Synthesis and preliminary evaluation of some 2-amino-n′-[substituted]-4,5,6,7-tetrahydro-1-benzothiophene-3-carbohydrazide as antimicrobial agents. *J. Pharm. Res.* **2015**, *9*, 10–14.
19. Mourey, R.J.; Burnette, B.L.; Brustkern, S.J.; Daniels, J.S.; Hirsch, J.L.; Hood Meyers, M.J.; Mnich, S.J.; Pierce, B.S.; Saabye, M.J.; Schindler, J.F.; et al. A benzothiophene inhibitor of mitogen-activated protein kinase-activated protein kinase 2 inhibits tumor necrosis factor α production and has oral anti-inflammatory efficacy in acute and chronic models of inflammation. *J. Pharmacol. Exp. Ther.* **2010**, *333*, 797–807. [CrossRef]
20. Rackham, M.D.; Brannigan, J.A.; Moss, D.K.; Yu, Z.; Wilkinson, A.J.; Holder, A.A.; Tate, E.W.; Leatherbarrow, R.J. Discovery of novel and ligand-efficient inhibitors of plasmodium falciparum and plasmodium vivax N-myristoyltransferase. *J. Med. Chem.* **2013**, *56*, 371–375. [CrossRef]
21. Bruker, A. *SAINT Software Reference Manual*; Bruker-AXS: Madison, WI, USA, 1998.
22. Spek, L.A. Single-crystal structure validation with the program PLATON. *J. Appl. Chem.* **2003**, *36*, 7–13.
23. Sheldrick, G.M. Crystal structure refinement with SHELXL. *Acta Cryst. C* **2015**, *71*, 3–8. [CrossRef] [PubMed]
24. Turner, M.J.; McKinnon, J.J.; Wolff, S.K.; Grimwood, D.J.; Spackman, P.R.; Jayatilaka, D.; Spackman, M.A. Crystal Explorer17, University of Western Australia. 2017. Available online: http://hirshfeldsurface.net (accessed on 15 February 2020).
25. Frisch, M.J.; Trucks, G.W.; Schlegel, H.B.; Scuseria, G.E.; Robb, M.A.; Cheeseman, J.R.; Scalmani, G.; Barone, V.; Mennucci, B.; Petersson, G.A.; et al. *GAUSSIAN 09. Revision A02*; Gaussian Inc.: Wallingford, CT, USA, 2009.
26. Keith, T.; Millam, J. *GaussView, Version 4.1, R. Dennington II*; Semichem Inc.: Shawnee Mission, KS, USA, 2007.
27. Reed, A.E.; Curtiss, L.A.; Weinhold, F. Intermolecular Interactions from a Natural Bond Orbital, Donor-Acceptor Viewpoint. *Chem. Rev.* **1988**, *88*, 899–926.
28. Islam, M.S.; Ghawas, H.M.; El-Senduny, F.F.; Al-Majid, A.M.; Elshaier, Y.A.; Badria, F.A.; Barakat, A. Synthesis of new thiazolo-pyrrolidine–(spirooxindole) tethered to 3-acylindole as anticancer agents. *Bioorg. Chem.* **2019**, *82*, 423–430. [CrossRef] [PubMed]
29. Barakat, A.; Islam, M.S.; Ghawas, H.M.; Al-Majid, A.M.; El-Senduny, F.F.; Badria, F.A.; Elshaier, Y.A.M.; Ghabbour, H.A. Substituted spirooxindole derivatives as potent anticancer agents through inhibition of phosphodiesterase 1. *RSC Adv.* **2018**, *8*, 14335–14346. [CrossRef]
30. Lotfy, G.; El Sayed, H.; Said, M.M.; Aziz, Y.M.A.; Al-Dhfyan, A.; Al-Majid, A.M.; Barakat, A. Regio-and stereoselective synthesis of new spirooxindoles via 1,3-dipolar cycloaddition reaction: Anticancer and molecular docking studies. *J. Photochem. Photobiol. B Biol.* **2018**, *180*, 98–108. [CrossRef]
31. Lotfy, G.; Said, M.M.; El Sayed, H.; El Sayed, H.; Al-Dhfyan, A.; Aziz, Y.M.A.; Barakat, A. Synthesis of new spirooxindole-pyrrolothiazole derivatives: Anti-cancer activity and molecular docking. *Biorg. Med. Chem.* **2017**, *25*, 1514–1523. [CrossRef]
32. Al-Majid, A.M.; Ghawas, H.M.; Islam, M.S.; Soliman, S.M.; El-Senduny, F.F.; Badria, F.A.; Ali, M.; Shaik, M.R.; Ghabbour, H.A.; Barakat, A. Synthesis of spiroindolone analogue via three components reaction of olefin with isatin and sarcosine: Anti-proliferative activity and computational studies. *J. Mol. Struct.* **2020**, *1204*, 127500. [CrossRef]
33. Lotfy, G.; Aziz, Y.M.A.; Said, M.M.; El Ashry, E.S.H.; El Tamany, E.S.H.; Barakat, A.; Ghabbour, H.A.; Yousuf, S.; Ul-Haq, Z.; Choudhary, M.I. Synthesis of oxindole analogues, biological activity, and in silico studies. *ChemistrySelect* **2019**, *4*, 10510–10516. [CrossRef]
34. Barakat, A.; Soliman, S.M.; Al-Majid, A.M.; Ali, M.; Islam, M.S.; Elshaier, Y.A.; Ghabbour, H.A. New spiro-oxindole constructed with pyrrolidine/thioxothiazolidin-4-one derivatives: Regioselective synthesis, x-ray crystal structures, hirshfeld surface analysis, dft, docking and antimicrobial studies. *J. Mol. Struct.* **2018**, *1152*, 101–114. [CrossRef]
35. Geerlings, P.; De Proft, F.; Langenaeker, W. Conceptual Density Functional Theory. *Chem. Rev.* **2003**, *103*, 1793–1874. [CrossRef]
36. Domingo, L.R.; Ríos-Gutiérrez, M.; Pérez, P. Applications of the Conceptual Density Functional Theory Indices to Organic Chemistry Reactivity. *Molecules* **2016**, *21*, 748. [CrossRef] [PubMed]
37. Foresman, J.B.; Frisch, A. *Exploring Chemistry with Electronic Structure Methods*, 2nd ed.; Gaussian: Pittsburgh, PA, USA, 1996.
38. Chang, R. *Chemistry*, 7th ed.; McGraw-Hill: New York, NY, USA, 2001.
39. Kosar, B.; Albayrak, C. Spectroscopic investigations and quantum chemical computational study of (E)-4-methoxy-2-[(*p*-tolylimino) methyl] phenol. *Spectrochim. Acta-Part A Mol. Biomol. Spectrosc.* **2011**, *78*, 160–167. [CrossRef] [PubMed]

40. Koopmans, T.A. Über die Zuordnung von Wellenfunktionen und Eigenwerten zu den einzelnen Elektronen eines Atoms. *Physica* **1934**, *1*, 104–113. [CrossRef]
41. Parr, R.G.; Yang, W. *Density Functional Theory of Atoms and Molecules*; Oxford University Press: Oxford, UK, 1989.
42. Parr, R.G.; Szentpaly, L.V.; Liu, S. Electrophilicity index. *J. Am. Chem. Soc.* **1999**, *121*, 1922–1924. [CrossRef]
43. Chamorro, E.; Pérez, P. Understanding the Reactivity of Captodative Ethylenes in Polar Cycloaddition Reactions. A Theoretical Study. *J. Org. Chem.* **2008**, *73*, 4615–4624.
44. Kumar, R.S.; Almansour, A.I.; Arumugam, N.; Althomili, D.M.Q.; Altaf, M.; Basiri, A.; Kotresha, D.; Manohar, T.S.; Venketesh, S. Ionic liquid-enabled synthesis, cholinesterase inhibitory activity, and molecular docking study of highly functionalized tetrasubstituted pyrrolidines. *Bioorg. Chem.* **2018**, *77*, 263–268. [CrossRef]